

Effect of hot extrusion and heat treatment on microstructure of nickel-base superalloy

Chen-ze LIU¹, Feng LIU^{1,2}, Lan HUANG¹, Liang JIANG¹

1. State Key Laboratory of Powder Metallurgy, Central South University, Changsha 410083, China;
2. School of Metallurgy and Environment, Central South University, Changsha 410083, China

Received 23 July 2013; accepted 12 May 2014

Abstract: Effects of hot extrusion (HEX) and heat treatment on prior particle boundary (PPB), MC carbides, γ' precipitates and grain size of nickel-base FGH96 superalloy were studied. The results show that PPB consists of large γ' , MC carbides enriched with Ti, Nb and a modicum of oxides. Thereafter, it can efficaciously tune γ' precipitate size from micrometer down to nanometer region and simultaneously results in the annihilation of PPB by HEX process. The activation energy for grain growth of as-HEXed FGH96 superalloy was measured to be 402.6 kJ/mol, indicating that γ' precipitate serves the critical role in inhibiting grain growth under sub-solvus heat treatment. Moreover, the results reveal that grain growth is primarily restrained by MC carbide in the case of super-solvus temperature.

Key words: nickel-base superalloy; carbide; prior particle boundary; hot extrusion; heat treatment

1 Introduction

Powder metallurgy (P/M) Ni-base superalloys are widely used in the aircraft engine owing to their superior high-temperature strength, creep and fatigue resistance [1–3]. Advanced superalloy FGH96 is processed using P/M route with exceptional mechanical properties in combination with microstructure stability up to 750 °C after a long-term exposure [4–8]. It is generally accepted that mechanical performance of superalloys is to a large extent governed by grain size, γ' precipitate, prior particle boundary (PPB), while these microstructure features can be significantly regulated by hot extrusion (HEX) and heat treatment process. Previous results [9–12] showed that PPB concentration can be only partially lowered by HIP together with heat treatment, whereas HEX process is an efficient method to completely eliminate PPB and refine grain size simultaneously [13–17]. Although HEX technique in superalloy is widely investigated, the PPB annihilation mechanism remains to be fully uncovered. Heat treatment technique offers a substantial route to alter the size, volume fraction, morphology of γ' precipitate. Whereas most of the aforementioned research work

focused on the effect of solution temperature, cooling rate, aging time on γ' precipitates [4,18], yet little work involved the role of precipitates in resisting grain growth of superalloys. Moreover, though carbides were thought to be ineffective for strengthening owing to their small amount volume fraction, carbides can markedly upgrade creep rate and rupture life through resisting grain boundary sliding. The heat treatment temperature was habitually chosen upon sub-solvus to avoid absolute dissolving of the γ' phase, and thus suppress abnormal grain growth [19]. To date, the previous work seldom mentioned the effect of carbide on the growth at super-solvus temperature.

This work aims to investigate the effect of HEX and heat treatment on the evolution of PPB, MC carbide, γ' precipitate of FGH96 superalloy. The development of γ' precipitate residing in PPB was particularly presented. The pinning effect of γ' precipitate and MC carbide on the grain growth was demonstrated.

2 Experimental

2.1 Phase transformation analysis and solvus temperatures determination

The element contents of the P/M nickel-base

Foundation item: Project (2012AA03A514) supported by the National High-Tech Research and Development Program of China; Project (2013M531803) supported by the Postdoctoral Science Foundation of China; Project (74341016096) supported by the Postdoctoral Science Foundation of Central South University, China; Project (2013RS4031) supported by the Hunan Provincial Science and Technology Plan, China

Corresponding author: Feng LIU; Tel: +86-18670324887; Fax: +86-731-88830938; E-mail: liufengehe@126.com

DOI: 10.1016/S1003-6326(14)63381-1

FGH96 superalloy (equivalent to René 88 DT alloy) are listed in Table 1. The equilibrium phase diagram of FGH96 was calculated by commercial software Thermo-Calc (Stockholm Sweden), as shown in Fig. 1, showing that the possible existent precipitations in the alloy are γ' , MC, $M_{23}C_6$, MB_2 , M_3B_2 , μ phase and σ phase. The theoretical γ' solvus temperature for the alloy was determined to be 1106 °C, corresponding to differential thermal analysis (DTA) experimental measurement [20–24]. Wherein, the solution temperature for MC carbide was calculated as high as 1300 °C, situating in the range between solidus (1266 °C) and liquidus (1350 °C). Such a high temperature leads to ultra-strong phase stability throughout heat treatment.

Table 1 Element contents of FGH96 superalloy (mass fraction, %)

Co	Cr	Mo	W	Al	Ti
13	16	4	4	2.1	3.7
Nb	B	Zr	C	Ni	
0.7	0.015	0.03	0.03	Bal.	

2.2 Material and experimental procedure

The superalloy powder was atomized by plasma rotation electric pole (PREP) technique with the oxygen content of 55×10^{-6} , and the average diameter was 108.29 μm . Subsequently, the powder was encapsulated in stainless steel sheath for hot isostatic pressing (150 MPa) at 1150 °C for 3 h. The HEX was performed at temperature of 1000 °C, extrusion force of 1.128×10^4 and extrusion velocity of 250 mm/s. The microstructures of all samples after HEX were observed along extrusion direction. Solution heat treatment was carried out in nitrogen protective quartz tube for 1 h and immediately water quenched.

2.3 Microstructure characterization

The samples were cut by electronic discharging machining and then embedded in the epoxy resin for mechanical grinding and polishing. Metallographic observation was performed by optical microscopy (Leica DM4000M) and SEM (FEI QuantaTM 650 FEG). The polished surface was etched using Kalling's reagent (5 g CuCl_2 , 100 mL HCl and 100 mL ethanol) for optical observation. Electron polishing (80 mL methanol and 60 mL HCl, 25–30 V) and electrolytic etching (170 mL H_3PO_4 , 16 g CrO_3 , 10 mL H_2SO_4 , 2–3 V) were utilized for further SEM characterization. Element partition was determined using electron probe microanalysis (EPMA, JXA-8530F), and electron backscatter diffraction (EBSD) was employed to map grain structure using the Oxford orientation imaging microscopy (OIM) system.

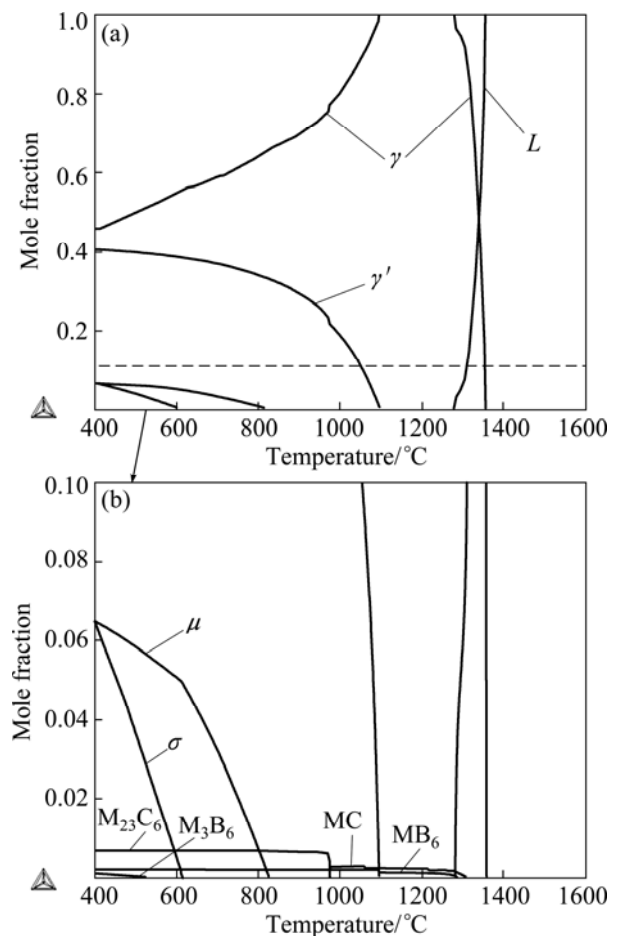


Fig. 1 Equilibrium phase diagram of FGH96 superalloy calculated by Thermo-Calc software (a) and closer-viewer on area in which mole fraction ranges from 0 to 0.1 (b)

3 Results and discussion

3.1 Microstructure and mechanisms of dynamic recrystallization

The as-HIPed FGH96 superalloy is fully compacted and consists of a myriad of exposed PPB, as shown in Fig. 2(a). The HIP process can completely homogenize the composition and eradicate the residual dendrites originated from the atomization process. Figure 2(b) shows that the grains are equiaxed with an average grain size of carbides located at spherical PPB substantial migration and then are reorganized in an aligned manner along extrusion direction. The size is 16 μm after HEX, in sharply contrast to 34 μm for as-HIPed condition. Surprisingly, ubiquitous PPB has entirely been removed by HEX, as validated by the absence of PPB in Fig. 2(b). Moreover, the EBSD images in Figs. 2(c) and (d) display the typical grain boundary morphologies from as-HIPed and as-HEXed, respectively. Wherein, both as-HIPed and as-HEXed show a majority of high angle boundary (black line) and only a small amount of low angle

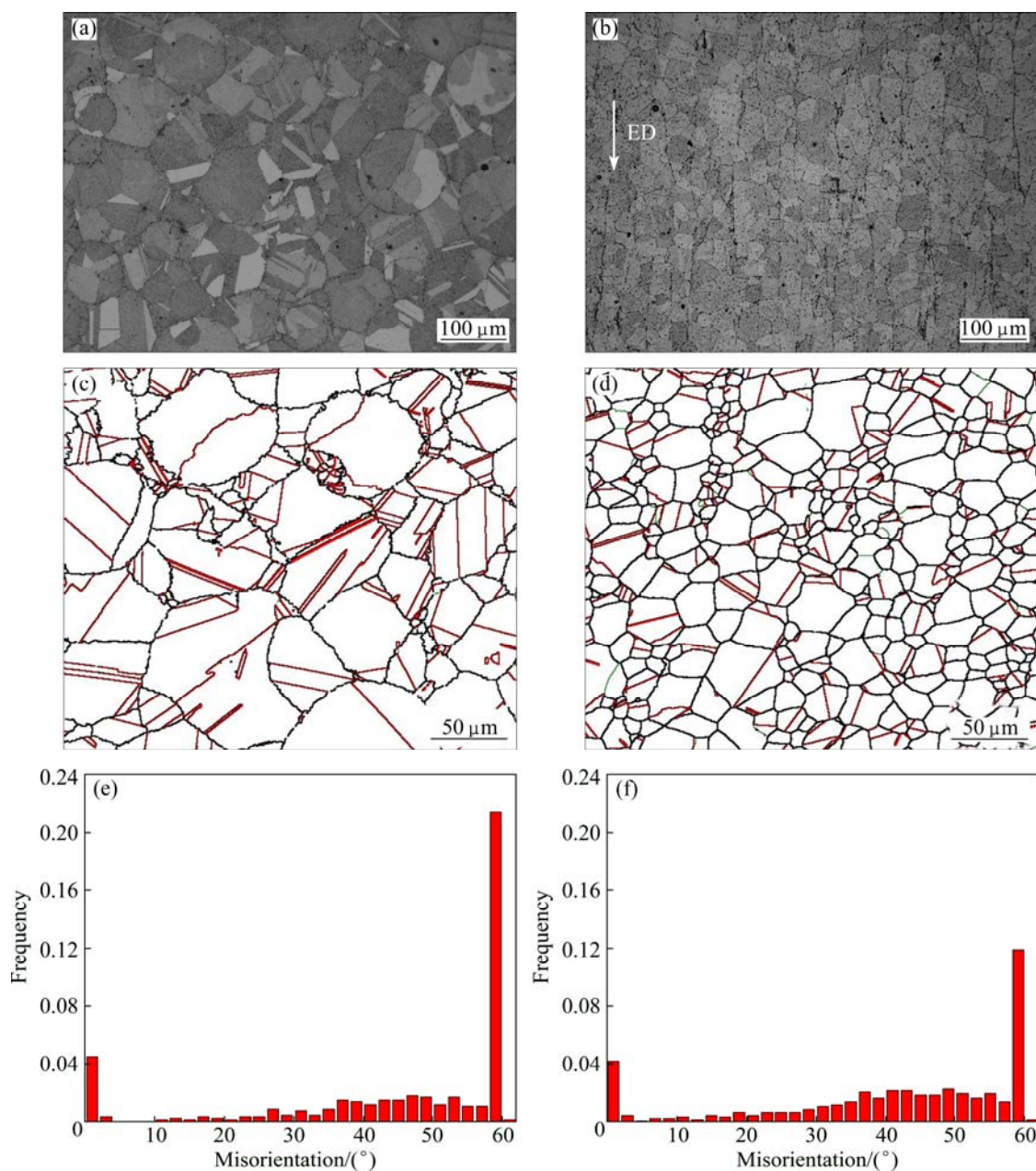


Fig. 2 Optical micrographs of as-HIPed alloy (a) and as-HEXed alloy (b), grain boundary morphologies of as-HIPed alloy (c) and as-HEXed alloy (d), grain boundary misorientation of as-HIPed alloy (e) and as-HEXed alloy (f)

boundaries (green line). Universal high angle grain boundary (Fig. 2(f)) indicates the occurrence of dynamic recrystallization (DRX), which is closely related to the strain-induced grain boundary migration. The DRX nucleation mechanism based on grain boundary microarchitecture can be attributed to discontinuous dynamic recrystallization (DDRX), although a small amount of low angle grain boundaries derived from continuous dynamic recrystallization (CDRX) exist in grain interior. It is worthy pointing out that the density of growth twinning (read line) attenuates from 42.5% to 22.4% due to the HEX effect, which can be compared in Figs. 2(e) and (f).

3.2 Evolution of PPB

The phase compositions of γ , γ' and carbide were calculated by Thermo-Calc software at 1000 °C considering HEX process was carried out upon 1000 °C (Table 2). In comparison to γ matrix, γ' precipitate is rich in Al, Ti, Ni, and MC carbide is rich in Ti, Nb, C. The results of EPMA shown in Fig. 3 reveal that continuous PPB after HIP process is decorated by large γ' precipitates (high concentration of Ni, Al and Ti), together with MC carbides (enrichment of Ti, Nb and C) situating in the vicinity of the large γ' and barely thin-film oxides (partition of Zr and O).

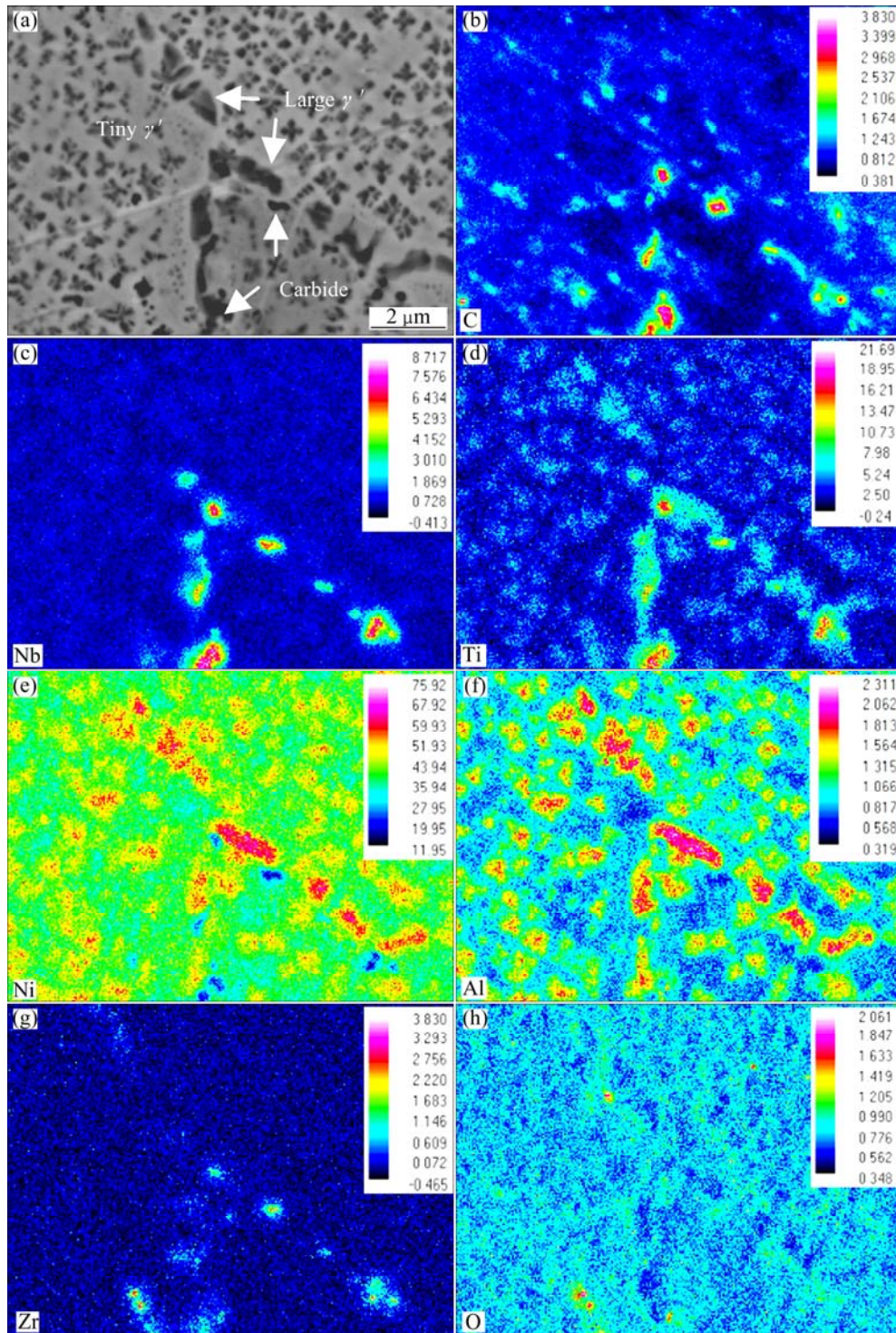
In contrast, the continuous PPB morphology is

Table 2 Element contents of γ , γ' and MC carbide at 1000 °C measured by Thermo-Calc software

Phase	Composition mass fraction/%										
	Co	Cr	Mo	W	Al	Ti	Nb	B	Zr	C	Ni
γ	14.5	19.7	4.9	4.6	1.4	1.8	0.3	–	–	–	52.8
γ'	7.8	2.3	0.3	1.6	4.8	10.4	1.9	–	–	–	70.9
MC	–	0.5	0.7	8.6	–	50.2	22.2	–	2.5	15.3	–

disrupted by HEX process, as shown in Fig. 4(a). Our EPMA results demonstrate that the carbide (white arrow in Fig. 4(a)) is heavily enriched with Ti, C and Nb (Figs. 4(b)–(d)), indicating that carbide composition remains unchanged even though HEX treatment is imposed. Yet, no Ni and Al is detected, revealing that large γ' precipitates are eliminated by severe plastic deformation during HEX.

The heat treated results at sub-solvus and super-

**Fig. 3** Element distribution mappings of as-HIPed alloy by EPMA

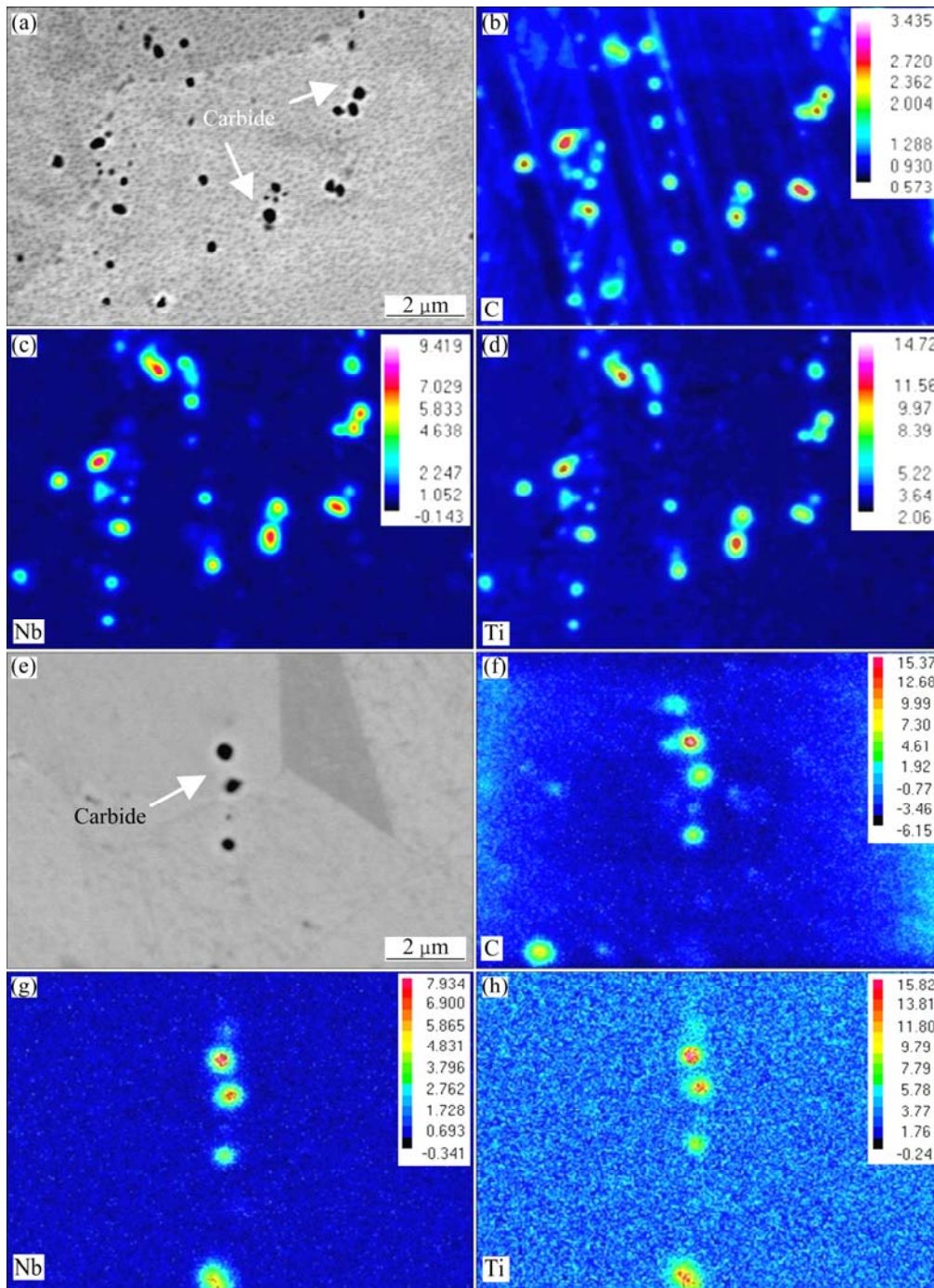


Fig. 4 Element distribution mappings of as-HEXed superalloy by EPMA

solvus temperatures validate that volume fraction and composition of MC carbide cannot be significantly modified by heat treatment. A representative solution treatment procedure at 1150 °C (super-solvus) is selected for EPMA back scattering observation (Fig. 4(e)), showing that MC carbide (white arrow in Fig. 4(e)) morphology and composition remains relatively stable.

Equilibrium thermodynamic measurements (Fig. 1) predict that MC carbide is microstructurally stable upon heat treatment in the vicinity of γ' solvus temperature. Meanwhile, the mole fraction of MC carbides is

calculated to be 0.26% at 1100 °C and it remains approximately stable between 980 and 1150 °C. The composition of MC carbides stays unchanged even though harsh solution treatment is executed, which is in good agreement with the EPMA results. Considering that MC is structurally stable up to 1300 °C, the MC carbides are not sensitive to solution-treatment temperature.

3.3 Development of γ' precipitates

The γ' precipitates (dark contrast particles in Fig. 5(a)), are $L1_2$ type (nominally Ni_3Al), exhibiting

irregular shapes and/or butterfly morphologies. Duplex morphologies of γ' precipitates located in the γ matrix and grain boundary after HIP process are readily observed, which is attributed from the fact that slow cooling during HIP process leads to the coarsening of γ' precipitates within the grain boundary compared to the uniform distribution of γ' precipitates in grain interior. Owing to the stress promotion in the process of HEX, γ' precipitate is accordingly refined and its shape ultimately evolves into close spherical morphology, as shown in Fig. 5(b). The thermodynamic interplay between recrystallization interface and original γ' precipitate can refine average grain size down to 16.1 μm and yield nanometer-sized γ' precipitates, respectively.

The γ' precipitate morphologies solution-treated at sub-solvus and super-solvus temperatures are shown in Figs. 5(c) and (d), respectively. The γ' precipitate coarsening upon sub-solvus treatment is clearly observed, and its morphology is eventually developed into nearly cuboidal after thermodynamic process. In contrast, γ' precipitate dissolves rapidly under super-solvus solution treatment, followed by the uniform precipitation of nanoscale γ' phase in the course of cooling. The fine and uniformly dispersed γ' precipitates are remarkably favorable for the mechanical strengthening of superalloys.

3.4 Effect of γ' precipitate and carbide on grain size

Five typical temperatures (950, 1000, 1050, 1100, and 1150 $^{\circ}\text{C}$) were selected for solution treatments after HEX process. The final average grain sizes were measured to be 17.9, 20.8, 25.1, 29.3 and 32.0 μm , respectively, well exceeding un-heat treated alloy, as shown in Fig. 6. These results indicate that the driving force of grain boundary migration is sufficiently high and overcomes the pinning force imposed by the γ' precipitates. However, abnormal grain growth is not witnessed, implying the resisting effect of γ' precipitates during heat treatment. Furthermore, super-solvus treatment promotes a moderate increase in the average grain size compared to sub-solvus condition. Clearly, super-solvus treatment provides relatively high temperature and facilitates grain coarsening due to the degrading of pinning force for γ' precipitate, yet no evident abnormal grain growth is found. While the solution temperature is elevated to 1200 $^{\circ}\text{C}$, anomalous grain growth and local fusion (Fig. 6(g)) arise because the temperature approaches solidus line.

Figure 7 shows the grain size distribution of HEXed specimens solution-treated at temperatures in the range of 950 to 1200 $^{\circ}\text{C}$. The reason why abnormal grain growth is not observed in the course of super-solvus

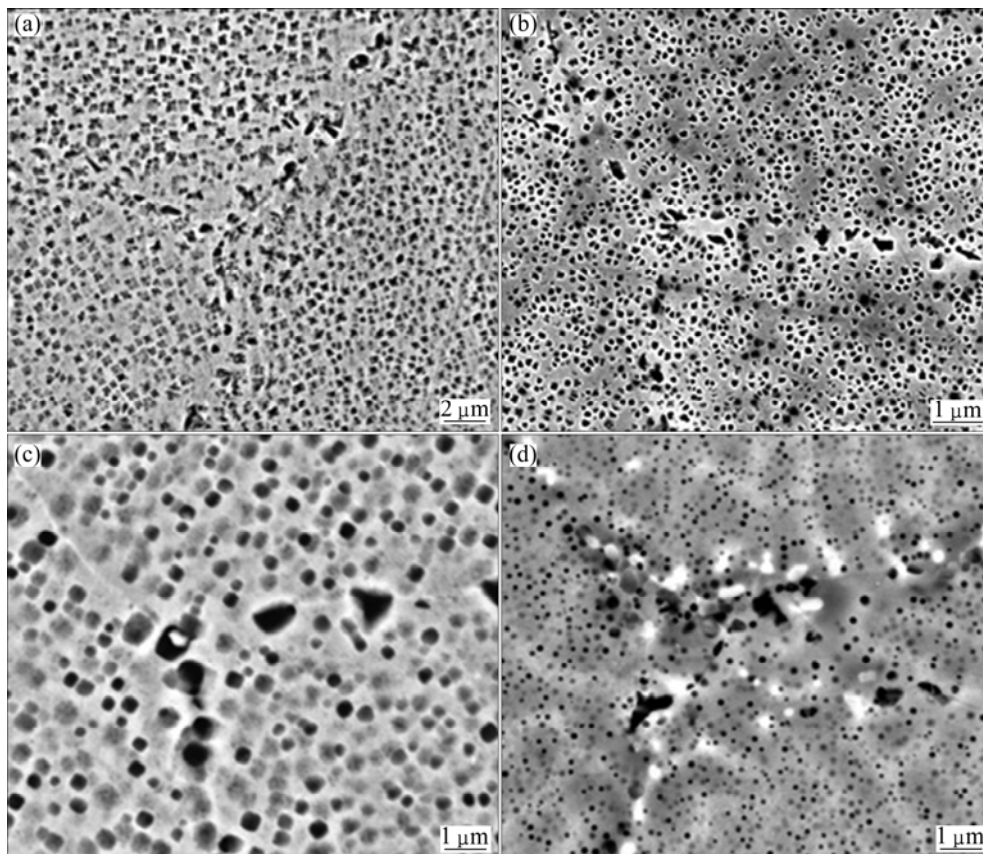


Fig. 5 SEM images of triple-point regions in FGH96 superalloy: (a) In condition of HIP; (b) After HEX; (c) Under sub-solvus treatment; (d) Under super-solvus treatment

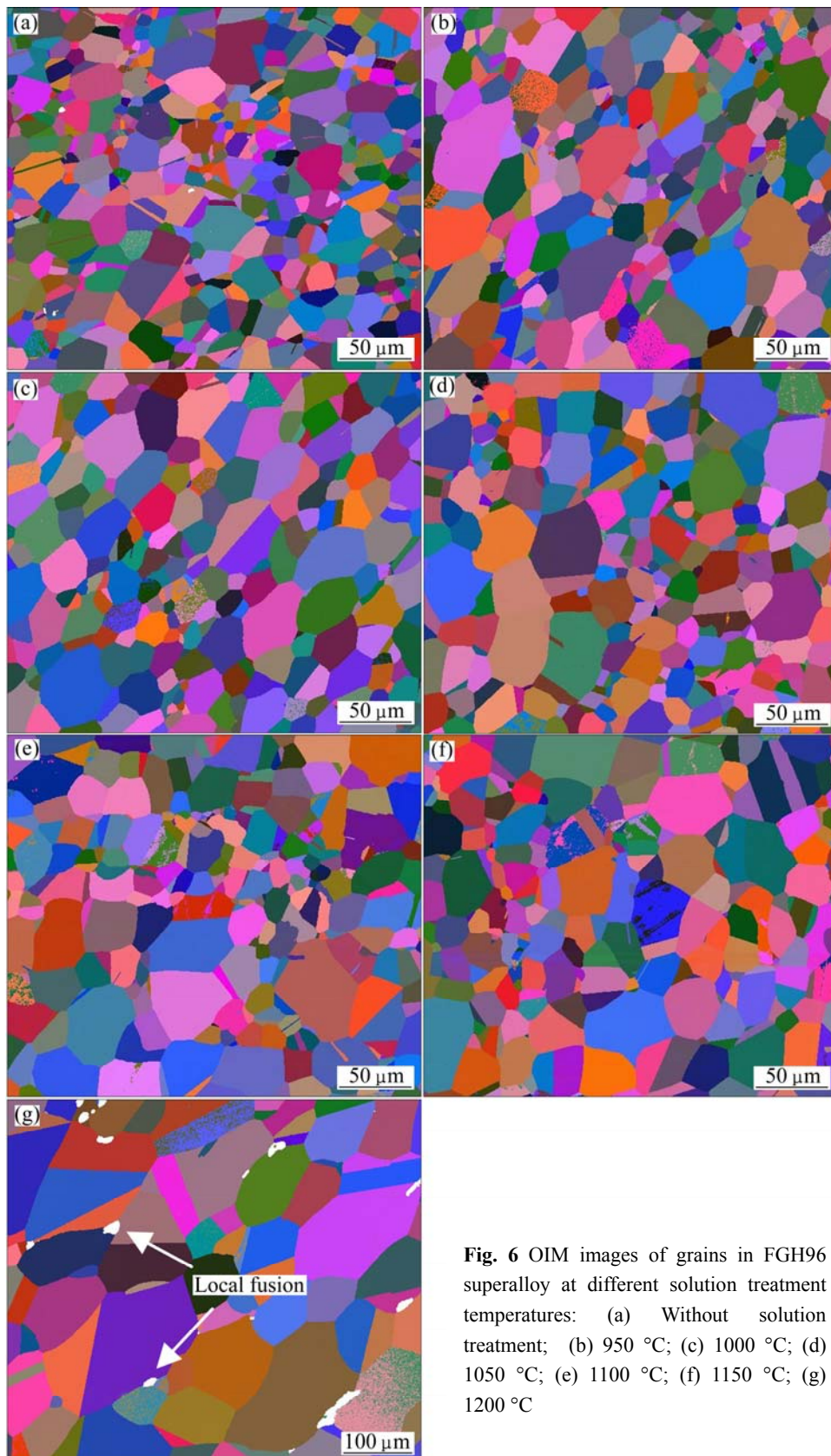


Fig. 6 OIM images of grains in FGH96 superalloy at different solution treatment temperatures: (a) Without solution treatment; (b) 950 °C; (c) 1000 °C; (d) 1050 °C; (e) 1100 °C; (f) 1150 °C; (g) 1200 °C

treatment will be discussed with reference to the corresponding γ' mole fractions and MC mole fractions calculated by Thermo-Calc. As the temperature increases,

the volume fraction of γ' decreases. Below γ' solvus temperature, the grain size increases slowly with increasing the temperature, but then increases more

observably as the γ' solvus temperature is approached. Upon super-solvus treatment, the dissolution of γ' precipitate is triggered, but the rate of grain growth shows comparatively under-sized increase. This indicates that MC carbide uniquely acts on pinning effect, which substantially hinders abnormal grain growth. Moreover, the explanation is strongly supported by previous conclusion [25] drawn from nickel-base superalloy Astroloy.

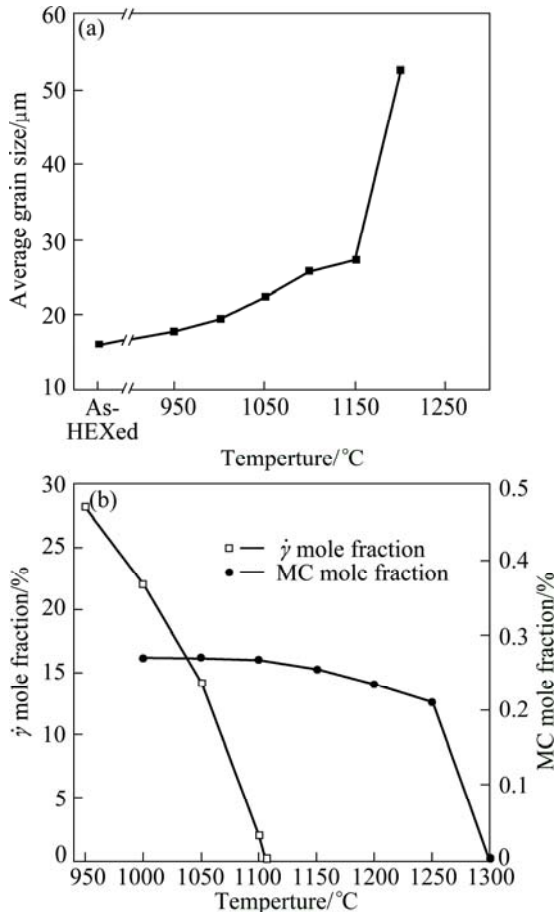


Fig. 7 Relationship between grain sizes (a), mole fraction of γ' , mole fraction (b) of MC carbides and solution treatment temperature

To further understand the role of γ' precipitates on the activation energy of grain growth, here the classical Sellars model [26] was adopted to establish the relationship between grain growth and heat-treatment temperatures as follows:

$$d^n = d_0^n + kt \exp\left(-\frac{Q}{RT}\right) \quad (1)$$

where d is the grown grain size; d_0 is the recrystallized grain size; t is the holding time; Q is the activation energy of grain growth; T is the heat treatment temperature; R is the universal gas constant; k and n are the material constants. Theoretically, n is estimated to be 2 for pure metal, and for grain growth data measured

over relatively long time equal to or in excess of 100 s and alloys with high alloying content, n value lies in the spectrum of 6 to 10. The activation energy for grain growth (Q) can be determined by

$$Q = \frac{\partial \ln(d^n - d_0^n)}{\partial(-1/T)} \times R \quad (2)$$

where n is measured to be 7.5 and the relationship between $\ln(d^{7.5} - d_0^{7.5})$ and $-1/T$ of solution-treated samples is shown in Fig. 8. The grain growth model for solution heat treatment after the HEX is given as

$$d^{7.5} = d_0^{7.5} + 6.1031 \times 10^{22} t \exp\left(-\frac{402600}{RT}\right) \quad (3)$$

For the duration of the holding period after HEX, the activation energy of grain growth is determined to be 402.6 kJ/mol, whereas the activation energy of pure nickel is 278 kJ/mol [27]. This indicates that the activation energy of grain growth is much higher than that of pure nickel because of the pinning effect of γ' phase on the grain boundary.

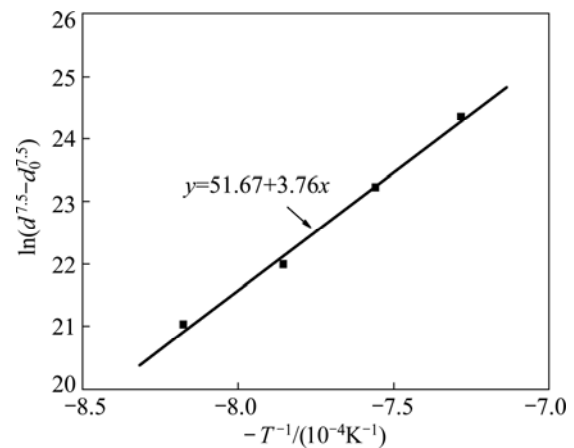


Fig. 8 Relationship between solution treatment temperature and grain size

4 Conclusions

1) In the case of HIP, continuous PPB is decorated with large γ' precipitates and MC carbides (enriched with Nb and Ti), as well as the small quantity of oxide. After HEX, γ' precipitate refinement can induce the annihilation of PPB, leading to excellent inter-particle bonding originated from hot deformation. Meanwhile, DDRX is the governing nucleation mechanism of DRX for FGH96 superalloy during HEX while CDRX acts as assisted role.

2) The activation energy of grain growth after HEX at sub-solvus is numerically determined to be 402.6 kJ/mol. Wherein, grain growth is significantly inhibited because of the pinning effect of γ' phase on grain boundary migration. Considering ultra-high stability of

MC carbide between solidus and liquidus, grain growth is extraordinarily impeded by carbide precipitate upon super-solvus treatment.

3) Super-solvus solution treatment offers an optimized γ' precipitate morphology and size, in conjunction with upgraded grain size distribution.

References

- [1] TILEY J, VISWANATHAN G B, HWANG J Y, SHIVELEY A, BANERJEE R. Evaluation of gamma prime volume fractions and lattice misfits in a nickel base superalloy using the external standard X-ray diffraction method [J]. *Materials Science and Engineering A*, 2010, 528(1): 32–36.
- [2] NING Yong-quan, YAO Ze-kun, Guo Hong-zhen, FU M W, LI Hui, XIE Xing-hua. Investigation on hot deformation behavior of P/M Ni-base superalloy FGH96 by using processing maps [J]. *Materials Science and Engineering A*, 2010, 527(26): 6794–6799.
- [3] HWANG J Y, BANERJEE R, TILEY J, SRINIVASAN R, VISWANATHAN G B, FRASER H L. Nanoscale characterization of elemental partitioning between gamma and gamma prime phases in rene 88 DT nickel-base superalloy [J]. *Metallurgical and Materials Transactions A*, 2009, 40(1): 24–35.
- [4] TILEY J, VISWANATHAN G B, SRINIVASAN R, BANERJEE R, DIMIDUK D M, FRASER H L. Coarsening kinetics of γ' precipitates in the commercial nickel base superalloy René 88 DT [J]. *Acta Materialia*, 2009, 57(8): 2538–2549.
- [5] VISWANATHAN G B, SAROSI P M, HENRY M F, WHITIS D D, MILLIGAN W W, MILLS M J. Investigation of creep deformation mechanisms at intermediate temperatures in René 88 DT [J]. *Acta Materialia*, 2005, 53(10): 3041–3057.
- [6] ZHANG Ming-jie, LI Fu-guo, CHEN Bo, WANG Shu-yun. Investigation of micro-indentation characteristics of P/M nickel-base superalloy FGH96 using dislocation-power theory [J]. *Materials Science and Engineering A*, 2012, 535: 170–181.
- [7] NING Yong-quan, YAO Ze-kun, LI Hui, GUO Hong-zhen, TAO Yu, ZHANG Yi-wen. High temperature deformation behavior of hot isostatically pressed P/M FGH4096 superalloy [J]. *Materials Science and Engineering A*, 2010, 527(4–5): 961–966.
- [8] NING Yong-quan, YAO Ze-kun, FU M W, GUO Hong-zhen. Dynamic recrystallization of the hot isostatically pressed P/M superalloy FGH4096 in hot working process [J]. *Materials Science and Engineering A*, 2010, 527(26): 6968–6974.
- [9] GAROSSHEN T. Influence of alloy chemistry on carbide precipitation in a nickel base superalloy [J]. *Metallurgical and Materials Transactions A*, 1986, 17(11): 2075–2077.
- [10] APPA RAO G, KUMAR M, SRINIVAS M, SARMA D S. Effect of standard heat treatment on the microstructure and mechanical properties of hot isostatically pressed superalloy inconel 718 [J]. *Materials Science and Engineering A*, 2003, 355(1–2): 114–125.
- [11] YU Jin-Jiang, SUN Xiao-Feng, ZHAO Nai-Ren, JIN Tao, GUAN Heng-Rong, HU Zhuang-Qi. Effect of carbon on microstructure and mechanical properties of DD99 single crystal superalloy [J]. *Transactions of Nonferrous Metals Society of China*, 2006, 16(s3): s1973–s1977.
- [12] YU Zhu-huan, LIU Lin, ZHANG Jun. Effect of carbon addition on carbide morphology of single crystal Ni-based superalloy [J]. *Transactions of Nonferrous Metals Society of China*, 2014, 24(2): 339–345.
- [13] CHANG D, KRUEGER D, SPRAGUE R. Superalloy powder processing, properties and turbine disk applications [J]. *Superalloys*, 1984: 245–273.
- [14] LU Yang-ling, LIU Jin-xi, LI Xiao-ke, LIANG Jian-ping, LI Zhi-jun, WU Guan-yuan, ZHOU Xing-tai. Hot deformation behavior of Hastelloy C276 superalloy [J]. *Transactions of Nonferrous Metals Society of China*, 2012, 22(s1): s84–s88.
- [15] GESSINGER G H, BOMFORD M. Powder metallurgy of superalloys [J]. *International Metallurgical Reviews* 1974, 19(1): 51–76.
- [16] CAI Da-yong, XIONG Liang-yin, LIU Wen-chang, SUN Gui-dong, YAO Mei. Characterization of hot deformation behavior of a Ni-base superalloy using processing map [J]. *Materials & Design*, 2009, 30(3): 921–925.
- [17] ZHANG Ming-jie, LI Fu-guo, WANG Shu-yun, LIU C Y. Effect of powder preparation technology on the hot deformation behavior of HIPed P/M nickel-base superalloy FGH96 [J]. *Materials Science and Engineering A*, 2011, 528(12): 4030–4039.
- [18] SINGH A R P, NAG S, CHATTOPADHYAY S, REN Y, TILEY J, VISWANATHAN G B, FRASER H L, BANERJEE R. Mechanisms related to different generations of γ' precipitation during continuous cooling of a nickel base superalloy [J]. *Acta Materialia*, 2013, 61(1): 280–293.
- [19] WU Yu-xiao, ZHANG Heng, LI Fu-lin, LI Shu-suo, GONG Sheng-kai, HAN Ya-fang. Kinetics and microstructural evolution during recrystallization of a Ni₃Al-based single crystal superalloy [J]. *Transactions of Nonferrous Metals Society of China*, 2012, 22(9): 2098–2105.
- [20] CHO Y K, YOON D Y, HENRY M F. The effects of deformation and pre-heat-treatment on abnormal grain growth in RENE 88 superalloy [J]. *Metallurgical and Materials Transactions A*, 2001, 32(12): 3077–3090.
- [21] TILEY J S, VISWANATHAN G B, SHIVELEY A, TSCHOPP M, SRINIVASAN R, BANERJEE R, FRASER H L. Measurement of γ' precipitates in a nickel-based superalloy using energy-filtered transmission electron microscopy coupled with automated segmenting techniques [J]. *Micron*, 2010, 41(6): 641–647.
- [22] WLODEK S, KELLY M, ALDEN D. The structure of Rene 88DT [J]. *Superalloys*, 1996: 129–136.
- [23] BURKE J J, WEISS V. *Powder metallurgy for high performance applications* [M]. New York: Syracuse University Press, 1972.
- [24] LI De-fu, GUO Qing-miao, GUO Shengli, PENG Hai-jian, WU Zhi-gang. The microstructure evolution and nucleation mechanisms of dynamic recrystallization in hot-deformed Inconel 625 superalloy [J]. *Materials & Design*, 2011, 32(2): 696–705.
- [25] WINBERG L, DAHLEN M. Recrystallization in a powder metallurgy nickel-base superalloy [J]. *Journal of Materials Science*, 1978, 13(11): 2365–2372.
- [26] DEVADAS C, SAMARASEKERA I, HAWBOLT E. The thermal and metallurgical state of steel strip during hot rolling: Part III. Microstructural evolution [J]. *Metallurgical and Materials Transactions A*, 1991, 22(2): 335–349.
- [27] KASHYAP B, CHATURVEDI M. Activation energy for superplastic deformation of IN718 superalloy [J]. *Scripta Materialia*, 2000, 43(5): 429–433.

热挤压及热处理对镍基高温合金 显微组织的影响

刘琛仄¹, 刘锋^{1,2}, 黄岚¹, 江亮¹

1. 中南大学 粉末冶金国家重点实验室, 长沙 410083;

2. 中南大学 冶金与环境学院, 长沙 410083

摘要: 研究热挤压以及热处理对镍基高温合金 FGH96 原始颗粒边界(PPB)、 γ' 相、MC 型碳化物及 γ 基体的影响。结果表明: PPB 是由大的 γ' 相、MC 型碳化物和少量的氧化物构成。可通过热挤压将 γ' 相尺寸由微米级细化到纳米级, 并达到消除 PPB 的效果。热挤压态 FGH96 合金的晶粒长大激活能为 402.6 kJ/mol, 表明在低于 γ' 相完全溶解的温度时, 晶粒长大受到 γ' 相的抑制。在稍高于 γ' 相完全溶解的温度时, MC 型碳化物起到钉扎晶界的作用并阻碍晶粒异常长大。

关键词: 镍基高温合金; 碳化物; 原始颗粒边界; 热挤压; 热处理

(Edited by Chao WANG)